Table 1 Characteristics of patients

	Stage of carpal tunnel syndrome			
	Control	Mild to moderate	Severe	Extreme
Number of patients	36	33	50	22
Age in years, mean (SD)	46.2 (7.2)	53.8 (10.8)	60.6 (13.0) p=0.015 v mild to moderate	64.4 (13.1) p=0.002 v mild to moderate
Wrist circumference in mm, mean (SD)	162.1 (8.6)	166.2 (7.1) p=0.036 v control	167.0 (12.3) p=0.044 v control	168.3 (16.9)
Wrist ratio	0.66 (0.03)	0.67 (0.04)	0.68 (0.04) p=0.030 v control	0.66 (0.04)
Duration of symptoms (months)		33.3 (52.3)	28.7 (43.3)	28.0 (44.7)
Side of the hand				
Right	36	7	29	11
Left	0	26	21	11
Surgery				
Yes	0	22	50	22
No	36	11	0	0

for T2; flip angle, 90° for T1 and 20° for T2; field of view, 12×12 cm; matrix, 192×256). Four axial image slices, perpendicular to the longitudinal line of the median nerve, were selected. Level 1 was at the distal part of the distal radioulnar joint level where the relative position of the ulnar head to the radial sigmoid notch varied due to difference in ulnar variance. Some subjects had ulnar plus variance, and others did not. We tried to select a slice that was closest to the distal sigmoid notch. Level 2 was at the middle of the pisiform. A slice that had the largest pisiform section was selected. Level 3 was at the hook of the hamate level. A slice with the longest hook of the hamate was selected. Level 4 was at the exit of the carpal tunnel. We had twelve slices for each wrist and attempted to select four slices for measurement that best met the above criteria.

Quantitative assessment was conducted for the cross sectional area, signal intensity ratio, and flattening ratio of the median nerve, flexor tendon area, carpal tunnel area, synovial area, and intersynovial space, palmar bowing of the TCL, circumference of the wrist, and wrist ratio, using NIH Image (version 1.61; National Institutes of Health), which is a public domain image processing and analysis program. The measurements were performed on the T2 image; however, when difficulties were encountered while delineating the structure, the T1 image was of help. The median nerve was traced at four levels as described by Monagle.[11] The signal intensity of the nerve was expressed as a ratio, which was calculated with respect to the signal intensity of the hypothenar muscles at level 4, to avoid variations in signal that are encountered with surface coils.[13] Thus, a value <1.0 means a higher intensity than the hypothenar muscle, and vice versa. The flattening ratio was calculated by dividing the transverse axis of the nerve by its longitudinal axis at the four levels. All flexor tendons inside the carpal tunnel, namely the flexor digitorum superficialis and profundus tendons and the flexor pollicis longus tendon, were traced at levels 2 and 3. The carpal tunnel area at level 2 was bounded anteriorly by the TCL, laterally by the capitotrapezial ligament and the

Table 2 Cross sectional area, signal intensity ratio and flattening ratio of the median nerve

	Level 1: DRUJ	Level 2: pisiform	Level 3: hook of the hamate	Level 4: distal TCL
Cross sectional area (mm^2)				
Control (n=36)	9.0 (2.5)	9.1 (2.3)	8.8 (1.8)	8.3 (2.0)
Mild to moderate (n=33)	14.1 (4.8)*	14.6 (4.8)*	10.8 (3.0)*	10.9 (3.2)*
Severe (n=50)	17.7 (6.7)* p=0.0085**	14.6 (5.6)*	11.2 (3.3)*	11.4 (3.5)*
Extreme (n=22)	19.5 (7.4)* p=0.0015**	14.8 (5.5)*	10.0 (3.1)	10.8 (3.2)*
Signal intensity ratio				
Control	3.31 (1.71)	3.14 (1.79)	3.16 (1.86)	3.47 (1.73)
Mild to moderate	2.08 (1.02)*	2.07 (1.02) p=0.0038*	2.54 (1.27)	2.50 (1.07) p=0.008*
Severe	1.45 (1.07)* p=0.0093**	1.86 (1.40)*	2.36 (1.44) p=0.026*	2.36 (1.41) p=0.0018*
Extreme	1.24 (0.58)* **	1.78 (1.40) p=0.0037*	2.43 (1.31)	2.35 (1.06) p=0.0086*
Flattening ratio				
Control	2.14 (0.41)	2.33 (0.52)	2.63 (0.67)	3.04 (0.70)
Mild to moderate	2.38 (0.61)	2.62 (0.55)* p=0.0245	2.76 (0.75)	2.87 (0.55)
Severe	2.56 (0.49)*	2.84 (0.55)*	2.53 (0.61)	2.77 (0.74)
Extreme	2.64 (0.42)*	2.92 (0.63)*	2.62 (0.87)	2.94 (1.19)

All values are expressed as means (SD).*p<0.05 vs control, **p<0.05 vs mild to moderate. The p value is not shown if <0.001. TCL, transverse carpal ligament.

Table 3 Palmar bowing of the TCL and cross sectional area of the flexor tendons, synovial space, and carpal tunnel

	Level 2: pisiform	Level 3: hook of the hamate
Flexor tendon area (mm^2)		
Control (n=36)	69.1 (7.7)	72.0 (8.6)
Mild to moderate (n=33)	76.4 (8.3)*	78.7 (8.2) p=0.0016*
Severe (n=50)	75.7 (9.6) p=0.001*	77.1 (9.3) p=0.0126*
Extreme (n=22)	74.6 (8.9) p=0.0157*	77.0 (10.6)
Synovial and intersynovial space (mm^2)		
Control	86.5 (13.3)	65.6 (8.0)
Mild to moderate	92.5 (14.4)	67.3 (12.2)
Severe	90.0 (15.0)	65.1 (10.7)
Extreme	84.8 (16.2)	63.0 (9.9)
Carpal tunnel area (mm^2)		
Control	164.6 (16.6)	146.3 (13.1) 136.4 (13.1)†
Mild to moderate	183.5 (16.8)*	156.8 (15.6) p=0.0035* 136.4 (17.5)†
Severe	180.3 (19.3)*	153.4 (15.4) p=0.0287* 132.2 (13.0)†
Extreme	174.2 (22.1)	150.0 (16.3) 131.1 (15.9)†
Palmar bowing (mm)		
Control		1.29 (0.78)
Mild to moderate		2.58 (0.82)*
Severe		2.78 (0.85)*
Extreme		2.26 (0.84)* p=0.0182**

All values are expressed as means (SD). *p<0.05 versus control, **p<0.05 versus severe. The p value is not shown if <0.001. †Carpal tunnel area in the absence of palmar bowing of the TCL. TCL, transverse carpal ligament.

scaphoid, medially by the pisiform, and dorsally by the carpal bones and the intercarpal ligament; that at level 3 was bounded anteriorly by the TCL, laterally by the capitotrapezial ligament and the scaphoid, medially by the hook of the hamate, and dorsally by the carpal bones and the intercarpal ligaments. The synovial area and intersynovial space were calculated by subtracting the flexor tendon area and median nerve area from the carpal tunnel area. The palmar bowing of the TCL was defined as the perpendicular distance to the TCL from the line between the hook of the hamate and the trapezium at level 3. The carpal tunnel area in the absence of palmar bowing of the TCL at level 3 was measured to assess the initial carpal tunnel area. The circumference of the wrist was measured at level 1 to assess wrist size. We calculated the wrist ratio by dividing the anteroposterior diameter by the transverse diameter at level 1. Each measurement described above was repeated three times, and the average values were used for data analysis. All measurements were rated by a single researcher (SU).

A small reproducibility exercise using pairs of repeated measurements on the median nerve cross sectional area at the level 1 of five patients showed no evidence of a systematic difference between occasions (paired t test $p = 0.6300$) and the intraclass correlation coefficient of 97.5% showed that errors of observation would contribute about 2.5% to the variation between subjects such as these. This reduced the sensitivity and power of the analyses, but not enough to matter with a sample of this size.

Severity of the disease was determined on the basis of nerve conduction velocities. This classification was similar to that of Padua *et al*[14] as follows. Normal: MDL <4.4 ms, SCV ≥44 m/s; mild: MDL <4.4 ms and SCV <44 m/s; moderate: MDL ≥4.4 ms and SCV <44 m/s; severe: MDL ≥4.4 ms and no response of SCV; extreme: no response of MDL and SCV. Based on the severity of the disease, the hands were classified into four groups: normal, mild to moderate CTS, severe CTS, and extreme CTS. The mild to moderate, severe, and extreme were regarded as CTS groups, and the normal group as the control.

Each parameter was compared between four different groups, using Student's t test. The correlation coefficient between the average area of the carpal tunnel at levels 2 and 3 and palmar bowing of the TCL was calculated, as was that between the circumference of the wrist and palmar bowing of the TCL for both the control and CTS groups. Statistical significance was achieved when the p value was <0.05.

RESULTS

Characteristics of the hands are shown in table 1. Carpal tunnel release surgery was performed on 94 wrists. Symptoms either disappeared or were relieved, and an improvement of nerve conduction velocities was confirmed after surgery.

Details of data of the cross sectional area, signal intensity ratio, and flattening ratio of the median nerve, the cross sectional area of the flexor tendons, synovium and intersynovial space, and the carpal tunnel, and the palmar bowing of the TCL are shown in tables 2 and 3.

In the control group, the cross sectional area of the median nerve and signal intensity ratio were constant throughout the levels, but flattening was more significant at level 4 than at the other levels. In the mild to moderate group, the cross sectional area was larger than in the control group in all slices, and the flattening ratio did not differ from the control group except at level 2. Cross sectional area at the proximal two levels was larger than at the distal two levels, and was accompanied by a lower signal intensity ratio (higher signal intensity) than the distal. In the severe and extreme groups, the cross sectional area was progressively larger proximally from level 3, and was accompanied by a high signal intensity. The flattening ratio was larger than the control group at levels 1 and 2. At level 3, the flattening ratio did not differ from the control group. Although the flexor tendon area and the carpal tunnel area were larger in the CTS groups than in the control group, significant differences were not detected among the CTS groups. Palmar bowing of the TCL was also greater in the CTS groups than in the control group, but the increase was less prominent in the extreme than in the severe group. No significant difference of synovial space and intersynovial area was detected among the groups. Figure 1 shows the carpal tunnel cross sections of the control, mild to moderate, and extreme groups.

A significant linear correlation between the average area of the carpal tunnel at levels 2 and 3 and palmar bowing of the TCL was noted for the CTS groups (correlation coefficient 0.489, $p<0.0001$), but not for the control group (0.154, $p = 0.374$). A significant correlation between the circumference of the wrist and palmar bowing of the TCL was not found for either the CTS or the control groups (0.067, $p = 0.497$ for the CTS; 0.16, $p = 0.353$ for the control).

When the carpal tunnel area was measured in the absence of palmar bowing of the TCL, no significant difference was detected among the groups ($p>0.1448$; table 3).

DISCUSSION

The aetiology of idiopathic CTS may be attributed to an incompatibility between the median nerve and carpal tunnel.[15 16] As a result, the intracarpal tunnel pressure increases,[17] and disturbance of circulation to the nerve occurs. Longstanding epineurial oedema leads to invasion of fibroblasts and subsequent formation of constricting scar

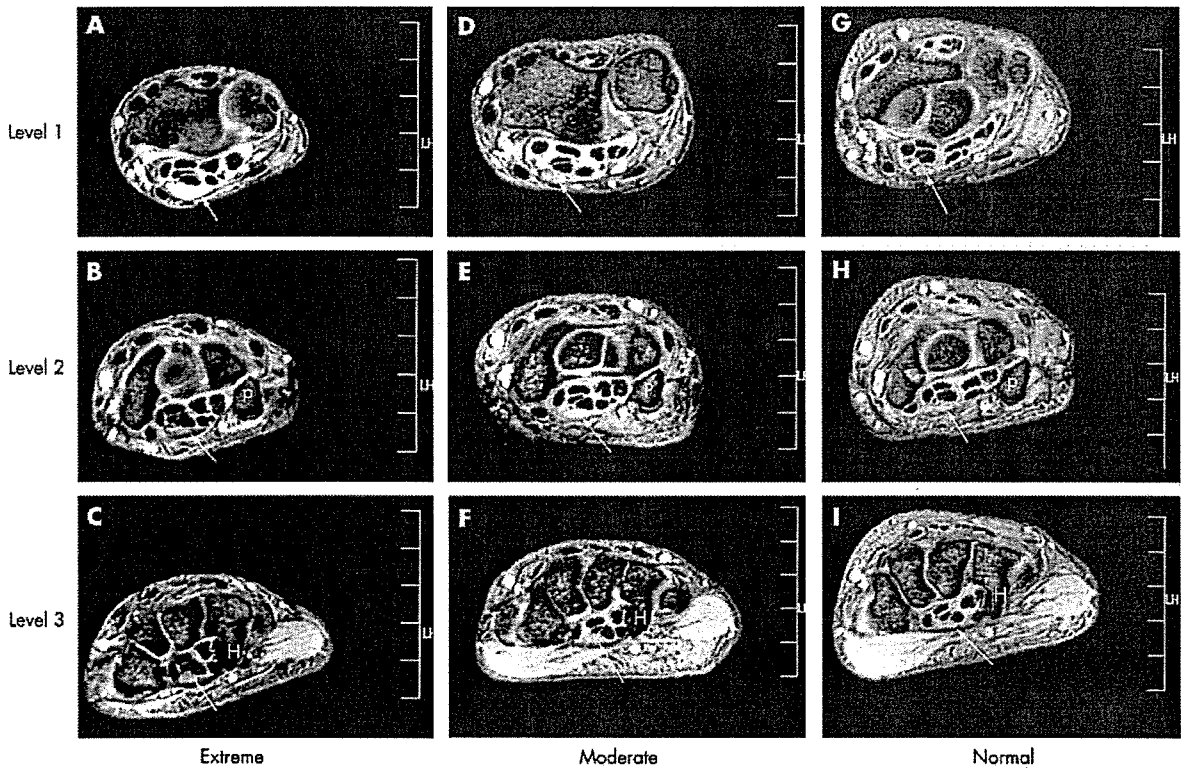

Figure 1 T2 weighted gradient echo images at the distal part of the distal radioulnar joint level (DRUJ) (1), at the level of the pisiform (2) and at the level of the hook of the hamate (3) in three different stages of idiopathic carpal tunnel syndrome. Solid arrow indicates the cross section of the median nerve. Upper part represents the dorsal side, and the righthand side represents the ulnar side. P, pisiform bone; H, hook of the hamate. (A–C) Extreme stage. Enlargement and high signal intensity of the flattened median nerve are seen at level 1, and enlargement of the median nerve at levels 2 and 3. Palmar bowing of the TCL is evident. (D–F) Moderate stage. Enlargement and high signal intensity of the median nerve are seen at level 2. They are slightly appreciated at level 3, and still not seen at level 1. Palmar bowing of the TCL is well appreciated. (G–I) Normal wrist. Enlargement of the median nerve is not seen at any level. Isointensity of the nerve to the hypothenar muscle is seen throughout the cross sections. Palmar bowing of the TCL is not seen.

tissue inside the nerve.[15] Swelling of the nerve trunk proximal to the compression site is due to an increase in the amount of endoneurial connective tissue,[18] oedema in the epineurium and endoneurial space, and obstruction of axoplasmic flow.[15] Macroscopic configuration of the median nerve during open carpal tunnel surgery has varied; however, conventionally proximal enlargement of the median nerve, or pseudoneuroma was believed to result from compression in the distal carpal tunnel, indicating a reduction in the size of the nerve or flattening of the nerve at the hook of the hamate level.[18–21]

Imaging techniques can be used to detect these morphological changes.[1 7] Using cadaveric specimens, MRI has been shown to be a valid and reproducible technique for measuring carpal tunnel volume and the cross sectional area of the flexor tendons and the median nerve.[22 23] Because the pathophysiology varies with the disease stage,[15] disease severity can affect the imaging outcome.[1 2]

Configuration of the median nerve is the parameter most widely investigated not only by MRI, but also by ultrasonography, because delineation of this nerve is easy. Enlargement of the cross sectional area of the median nerve at the proximal carpal tunnel or at the entrance to the tunnel was found to be of diagnostic value for idiopathic CTS in the majority of cases studied.[1 3 4 7 11 13 24 25] However, several investigators have shown a larger cross sectional area of the nerve in CTS groups than in controls.even at the hook of the hamate level[4 7 11] Kleindienst *et al* demonstrated that oedema of the nerve resulted in pre-stenotic swelling and moderate intracarpal swelling, and that the advanced stages of CTS showed retrograde swelling of the median nerve more than the earlier stages.[25] Our results were nearly consistent with these results.

There have been inconsistencies in results regarding the flattening ratio of the median nerve among investigators. Some found no difference between the idiopathic CTS groups and controls;[11 26] however, others have shown that the median nerve was more flattened at the level of the hook of the hamate in CTS groups than in control subjects.[4 7 13] In our study, no significant difference was detected at this level, but the large standard deviation of the flattening ratio indicated that the median nerve configuration varied even within the same disease stage, indicating that the median nerve did not always have a compressive deformity at this level. The median nerve was flattened at the level of exit of the TCL for all CTS groups and the control group, because furcation of the nerve could be observed at this level. Our results suggest that inconsistencies among previous studies in the flattening ratio were due to differences in patient spectra or pathophysiology, or both.

T2 MRI presents the normal nerve as isointensity, and it may develop a high signal intensity when it is damaged or degenerated.[27 28] The increased nerve signal on T2 MRI is due to interstitial oedema and the collapse and loss of myelinated fibres.[29] Preoperative high signal intensity of the median nerve on T2 may be a meaningful finding for idiopathic CTS,

because it decreases after surgical decompression of the nerve.[4 5 13 30] Because the signal intensity ratio was found to be inversely proportional to the area of the median nerve, the enlargement of the median nerve was associated with higher water content or more degeneration inside the nerve than in the normal nerve. Bulbous swelling of the median nerve at the level proximal to the carpal tunnel that is often observed during surgeries could be a characteristic finding of the advanced stages of the disease. In our study, this swelling was often accompanied by higher signal intensity than the distal level, suggesting oedema and degeneration of the nerve. However, signal intensity could be decreased in the advanced CTS because of fibrosis within the nerve.[25]

Quantification of the flexor tendon area was only performed in studies by Monagel and Cobb.[11 31] Monagel found no differences in the flexor tendon area between CTS patients and normal subjects.[11] Cobb *et al* showed increased carpal tunnel contents (flexor tendon and median nerve) to carpal tunnel volume ratios in CTS compared with controls.[31] As the number of hands analysed was small in both studies, no definitive conclusions could be made. In our study, we were not sure if the enlargement of the flexor tendons was congenital, or the result of the disease. Differences in flexor tendon size between CTS groups and control subjects remain to be clarified.

Phalen believed that thickening or fibrosis of the synovium was the main cause of idiopathic CTS.[20] This is believed to be due to an increased volume of the carpal tunnel contents or the result of swelling by repetitive motion of the digits, which leads to chronic tenosynovial thickening and fibrosis.[32] Britz *et al*[5] and Zagnoli *et al*[8] assessed the synovium inside the carpal tunnel by evaluating the interspace or the distance between the flexor tendons by MRI. Their studies involved a qualitative analysis, and interobserver variation was found to be considerable. We did not find any differences in area between the CTS groups and the control group. However, with our method it was difficult to evaluate subtle changes of synovium or subsynovial connective tissue, which may have an important role in development of idiopathic CTS.[33]

The size of the carpal tunnel area has been measured by MRI and CT, but the results were inconsistent. Some showed a larger carpal tunnel area in patients than in controls,[34] but others did not.[3 35 36] Our result indicated that the area at the proximal and the distal carpal tunnel was significantly larger in all groups except in the extreme group than it was in the control group. Previous investigators believed that palmar bowing of the TCL was greater in idiopathic CTS groups than in the control subjects.[4 7 8 11] Our result was consistent with that belief. In such cases, some structure inside the carpal tunnel is needed to push the TCL in a volar direction. However, few studies have correlated this parameter with the carpal tunnel area. Monagel *et al* did not find any difference between carpal tunnel areas, but showed that palmar bowing differed between the CTS and control groups.[11] We showed a significant linear correlation between the area of the carpal tunnel and palmar bowing of the TCL for the CTS groups, but not for the control group. Furthermore, palmar bowing of the TCL did not have a linear correlation with wrist size in either group. These results suggest that increased palmar bowing of the TCL is a characteristic of idiopathic CTS, resulting from an increase in the area of the carpal tunnel. It may be a result of the disease, not a difference in the initial carpal tunnel area, as the carpal tunnel area in the absence of palmar bowing of the TCL of the CTS groups was the same as that of the control group. The increased area of the carpal tunnel could be due to flexor tendons and the median nerve. Because synovial evaluation was difficult to perform in this study, the involvement of the synovium with enlargement of the carpal tunnel remains to be clarified.

Palmar bowing of the TCL could also be useful to assess disease severity because it was less prominent in the extreme than the severe group. This may be due to decreased tissue swelling such as swelling of the median nerve inside the carpal tunnel, as severity progresses, because the median nerve area and the carpal tunnel area of the extreme group was not as large as in the other CTS groups at the level of the hook of the hamate.

Based on this study, which quantitatively analysed the largest number of female subjects ever examined, the increased palmar bowing of the TCL was found to be due to an increase in the area of the carpal tunnel in idiopathic CTS. Although enlargement of the carpal tunnel area and the flexor tendon area could be characteristic findings for idiopathic CTS on T2 MRI, severity of the disease was difficult to judge using those parameters. It could be best judged by evaluating palmar bowing of the TCL and longitudinal changes in signal intensity and in the configuration of the median nerve.

This study may explain the reason for inconsistencies in previous studies and help to elucidate the pathophysiology of idiopathic CTS. However, there are some limitations to this study. As some variations were observed within the same group, there could be differences in pathophysiology inside the carpal tunnel of individuals, even in a relatively uniform group of subjects, all of whom were clinically diagnosed with idiopathic CTS. It would have been better to enrol patients with minimum neurophysiological abnormalities such as Padua's minimal stage,[14] because much of the remaining uncertainty over the use of imaging in CTS concerns whether imaging modalities add anything when the neurophysiological abnormalities are minimal. The effect of aging on changes of the median nerve and flexor tendon configuration has not been studied by MRI, and high signal intensity on T2 images could not be always specific. Because we performed endoscopic carpal tunnel release in many patients in this study, we did not correlate the status of the structures inside the carpal tunnel during surgery with the preoperative MRI. The many statistical tests could cause some significant findings to arise by chance, thus the p values should simply be used as an indication of the strength of a particular piece of evidence.

ACKNOWLEDGEMENT

We thank Dr K Yamashita Department of Radiology, Suwa Red Cross Hospital, for his advice on the MRI protocol and on the interpretation of images, and also Mr T Muramatsu, Imaging Technology Center, Suwa Red Cross Hospital, for his effort to improve the quality of the MRI of the wrist. We thank the nurses in Suwa Red Cross Hospital for their willingness to participate in this study.

Authors' affiliations
S Uchiyama, T Itsubo, H Nakagawa, M Kamimura, Department of Orthopaedic Surgery, Suwa Red Cross Hospital, Suwa City, Japan
T Yasutomi, Department of Orthopaedic Surgery, Shiokawa Hospital, Sutama, Japan
H Kato, Department of Orthopaedic Surgery, Shinshu University School of Medicine, Matsumoto City, Japan

Competing interests: none declared

REFERENCES

1 **Nakamichi K,** Tachibana S. Enlarged median nerve in idiopathic carpal tunnel syndrome. *Muscle Nerve* 2000;**23**:1713–18.
2 **Pasternack II,** Malmivaara A, Tervahartiala P, *et al.* Magnetic resonance imaging findings in respect to carpal tunnel syndrome. *Scand J Work Environ Health* 2003;**29**:189–96.
3 **Jarvik JG,** Yuen E, Haynor DR, *et al.* MR nerve imaging in a prospective cohort of patients with suspected carpal tunnel syndrome. *Neurology* 2002;**58**:1597–602.
4 **Allmann KH,** Horch R, Uhl M, *et al.* MR imaging of the carpal tunnel. *Eur J Radiol* 1997;**25**:141–5.

5 **Britz GW**, Haynor DR, Kuntz C, *et al.* Carpal tunnel syndrome:correlation of magnetic resonance imaging, clinical, electrodiagnostic, and intraoperative findings. *Neurosurgery* 1995;**37**:1097–103.
6 **Deryani E**, Aki S, Muslumanoglu L, *et al.* MR imaging and electrophysiological evaluation in carpal tunnel syndrome. *Yonsei Med J* 2003;**44**:27–32.
7 **Mesgarzadeh M**, Triolo J, Schneck CD. Carpal tunnel syndrome. MR imaging diagnosis. *Magn Reson Imaging Clin N Am* 1995;**3**:249–64.
8 **Zagnoli F**, Andre V, Dreff PL, *et al.* Idiopathic carpal tunnel syndrome. Clinical, electrodiagnostic, and magnetic resonance imaging correlations. *Rev Rhum* 1999;**66**:192–200.
9 **Treaster DE**, Burr D. Gender differences in prevalence of upper extremity musculoskeletal disorders. *Ergonomics* 2004;**47**:495–526.
10 **Dekel S**, Papaioannou T, Rushworth G, *et al.* Idiopathic carpal tunnel syndrome caused by carpal stenosis. *BMJ* 1980;**280**:1297–9.
11 **Monagle K**, Dai G, Chu A, *et al.* Quantitative MR imaging of carpal tunnel syndrome. *AJR* 1999;**172**:1581–6.
12 **Uchiyama S**, Toriumi H, Nakagawa H, *et al.* Postoperative nerve conduction changes after open and endoscopic carpal tunnel release. *Clin Neurophysiol* 2002;**113**:64–70.
13 **Cudlip SA**, Howe FA, Clifton A, *et al.* Magnetic resonance neurography studies of the median nerve before and after carpal tunnel decompression. *J Neurosurg* 2002;**96**:1046–51.
14 **Padua L**, LoMonaco M, Gregori B, *et al.* Neurophysiological classification and sensitivity in 500 carpal tunnel syndrome hands. *Acta Neurol Scand* 1997;**96**:211–17.
15 **Lundborg G**. Nerve entrapment. In: Lundborg G, ed. *Nerve injury and repair.* Edinburgh London Melbourne and New York: Churchill Livingstone, 1988:102–48.
16 **Hart AM**, Wiberg M. Nerve compression or mechanical neuropathy: neuropathology. *Curr Orthopaed* 2001;**15**:245–8.
17 **Gelberman RH**, Hergenroeder PT, Hargens AR, *et al.* The carpal tunnel syndrome. A study of carpal canal pressures. *J Bone Joint Surg* 1981;**63A**:380–3.
18 **Thomas PK**, Fullerton PM. Nerve fibre size in the carpal tunnel syndrome. *J Neurol Neurosurg Psychiatry* 1963;**26**:520–27.
19 **Goodman HV**, Gilliatt RW. The effect of treatment on median nerve conduction in patients with the carpal tunnel syndrome. *Ann Phys Med* 1961;**6**:137–55.
20 **Phalen GS**. The carpal-tunnel syndrome: seventeen years' experience in diagnosis and treatment of six hundred fifty-four hands. *J Bone Joint Surg* 1966;**48A**:211–28.
21 **Tanzer RC**. The carpal tunnel syndrome: a clinical and anatomical study. *J Bone Joint Surg* 1959;**41A**:624–34.
22 **Richman JA**, Gelberman RH, Rydevik BL, *et al.* Carpal tunnel volume determination by magnetic resonance imaging three-dimensional reconstruction. *J Hand Surg* 1987;**12A**:712–17.
23 **Cobb TK**, Dalley BK, Posteraro RH, *et al.* Establishment of carpal contents/canal ratio by means of magnetic resonance imaging. *J Hand Surg* 1992;**17A**:843–9.
24 **Kele H**, Verheggen R, Bittermann HJ, *et al.* The potential value of ultrasonography in the evaluation of carpal tunnel syndrome. *Neurology* 2003;**61**:389–91.
25 **Kleindienst A**, Hamm B, Lanksch WR. Carpal tunnel syndrome: staging of median nerve compression by MR imaging. *JMRI* 1998;**8**:1119–25.
26 **Bak L**, Bak S, Gaster P, *et al.* MR imaging of the wrist in carpal tunnel syndrome. *Acta Radiol* 1997;**38**:1050–2.
27 **Dailey AT**, Tsuruda JS, Filler AG, *et al.* Magnetic resonance neurography of peripheral nerve degeneration and regeneration. *Lancet* 1997;**350**:1221–2.
28 **Teresi LM**, Hovda D, Seeley AB, *et al.* MR imaging of experimental demyelination. *Am J Radiol* 1989;**152**:1291–8.
29 **Does MD**, Snyder RE. Multiexponential T2 relaxation in degenerating peripheral nerve. *Magn Reson Imaging* 1996;**35**:207–13.
30 **Pierre-Jerome C**, Bekkelund SI, Mellgren SI, *et al.* Bilateral fast magnetic resonance imaging of the operated carpal tunnel. *Scand J Plast Reconstr Hand Surg* 1997;**31**:171–7.
31 **Cobb TK**, Bond JR, Cooney WP, *et al.* Assessment of the ratio of carpal contents to carpal tunnel volume in patients with carpal tunnel syndrome: a preliminary report. *J Hand Surg* 1997;**22A**:635–9.
32 **Shum C**, Parisien M, Strauch RJ, *et al.* The role of flexor tenosynovectomy in the operative treatment of carpal tunnel syndrome. *J Bone Joint Surg* 2002;**84A**:221–5.
33 **Ettema AM**, Amadio PC, Zhao C, *et al.* A histological and immunohistochemical study of the subsynovial connective tissue in idiopathic carpal tunnel syndrome. *J Bone Joint Surg* 2004;**86A**:1458–66.
34 **Winn FJ Jr**, Habes DJ. Carpal tunnel area as a risk factor for carpal tunnel syndrome. *Muscle Nerve* 1990;**13**:254–8.
35 **Bleecker ML**, Bohlman M, Moreland R, *et al.* Carpal tunnel syndrome:role of carpal canal size. *Neurology* 1985;**35**:1599–604.
36 **Pierre-Jerome C**, Bekkelund SI, Mellgren SI, *et al.* Quantitative MRI and electrophysiology of preoperative carpal tunnel syndrome in a female population. *Ergonomics* 1997;**40**:642–9.

Available online at www.sciencedirect.com

SCIENCE DIRECT

Advanced Drug Delivery Reviews 57 (2005) 1037–1048

Advanced DRUG DELIVERY Reviews

www.elsevier.com/locate/addr

Synthetic biodegradable polymers as drug delivery systems for bone morphogenetic proteins

N. Saito[a,*], N. Murakami[b], J. Takahashi[b], H. Horiuchi[b], H. Ota[b], H. Kato[b], T. Okada[c], K. Nozaki[d], K. Takaoka[e]

[a]*Department of Physical Therapy, Shinshu University School of Health Sciences, 3-1-1 Asahi, Matsumoto, Nagano 390-8621, Japan*
[b]*Department of Orthopaedic Surgery, Shinshu University School of Medicine, 3-1-1 Asahi, Matsumoto, Nagano 390-8621, Japan*
[c]*Research Institute, Taki Chemical Co., Ltd., 64-1 Nishiwaki, Befucho, Kakogawa, Hyogo 675-0125, Japan*
[d]*Applied Pharmacology Laboratories, Institute for Drug Discovery Research, Yamanouchi Pharmaceutical Co., Ltd., 21 Miyukigaoka, Tsukuba, Ibaraki 305-8585, Japan*
[e]*Department of Orthopaedic Surgery, Osaka City University Graduate School of Medicine, 1-5-7 Asahimachi, Abeno-ku, Osaka 545-0051, Japan*

Received 8 April 2004; accepted 30 December 2004

Abstract

Bone morphogenetic proteins (BMP) induce bone formation in vivo, and clinical application in repair of bone fractures and defects is expected. However, appropriate systems to deliver BMP for clinical use need to be developed. We synthesized a new synthetic biodegradable polymer, poly-D,L-lactic acid-para-dioxanone-polyethylene glycol block copolymer (PLA-DX-PEG), to serve as a biocompatible, biodegradable polymer for recombinant human (rh) BMP-2 delivery systems. In animal experiments, new bone was efficiently formed and a large bone defect was repaired using PLA-DX-PEG/rhBMP-2 composites. In addition, this new polymer could be used as an injectable delivery system for rhBMP-2. The rhBMP-2/PLA-DX-PEG composites also could be combined with other materials such as hydroxyapatite or titanium. This new synthetic polymer might be used for rhBMP-2 delivery in various clinical situations involving repair of bone, leading to great changes in orthopedic treatment.

Keywords: Bone formation; Bone repair; Fracture; Bone defect; Recombinant human bone morphogenetic protein-2; Tissue engineering

* Corresponding author. Tel./fax: +81 263 37 2409.
E-mail address: saitoko@hsp.md.shinshu-u.ac.jp (N. Saito).

0169-409X/$ - see front matter © 2005 Elsevier B.V. All rights reserved.
doi:10.1016/j.addr.2004.12.016

Contents

1. Introduction . . . 1038
2. Bone morphogenetic proteins (BMP) and delivery systems . . . 1038
2.1. BMP . . . 1038
2.2. Delivery systems for BMP . . . 1039
2.3. Synthetic polymers for BMP delivery system . . . 1039
3. Development of new synthetic biodegradable polymers for rhBMP-2 delivery . . . 1040
3.1. Poly-D,L-lactic acid-polyethylene glycol block copolymer (PLA-PEG) . . . 1040
3.2. Poly-D,L-lactic acid-para-dioxanone-polyethylene glycol block copolymer (PLA-DX-PEG) . . . 1040
4. Repair of bone tissues using rhBMP-2 and new synthetic polymers . . . 1042
4.1. Repair of bone defect using composites of rhBMP-2 and synthetic polymers . . . 1042
4.2. Injectable polymeric delivery systems for rhBMP-2 . . . 1043
4.3. Combination of the rhBMP-2/polymer composites with other materials . . . 1044
4.4. Development of a new artificial joint that restores a bone defect . . . 1045
5. Conclusions . . . 1045
Acknowledgements . . . 1046
References . . . 1046

1. Introduction

The regeneration potential of human bone appears to be limited, given that repair of large bone defects such as those associated with comminuted fractures or bone tumor resection usually remains unrepaired [1]. Such cases have been treated routinely with autogeneic or allogeneic bone grafting. Major problems associated with autogeneic grafting include limited anatomic sources of donor bone and risk of morbidity from the additional surgery for procurement of the graft. In allogeneic bone grafting, major concerns are potential risks of transmission of disease, immunologic reaction of the host, poor osteogenic capacity of the transplanted bone, and high costs associated with a bone banking system [2–4]. Current examination of alternatives to grafting techniques suggests three possible new approaches to inducing new bone formation: implantation of certain cytokines such as bone morphogenetic proteins (BMP) in combination with appropriate delivery systems at the target site [5–7]; transduction of genes encoding cytokines with osteogenic capacity into cells at repair sites [8,9]; and transplantation of cultured osteogenic cells derived from host bone marrow [10–13]. In our estimation, the second approach represents the next major advance, while the third requires considerable additional resources and time to procure and culture cells. The first strategy appears to show the most practical promise for the near future. Appropriate delivery systems are essential to this technique. In this review, we outline the development of new delivery systems for BMP and preclinical animal experiments concerning bone tissue regeneration that suggest clinical applications.

2. Bone morphogenetic proteins (BMP) and delivery systems

2.1. BMP

BMP induce new bone formation by directing mesenchymal stem cells toward chondroblastic and osteoblastic differentiation, and causing them to proliferate in vivo. BMP expression has been confirmed to occur at the initial stage of the fracture healing process, and to participate in a cascade regulating bone repair processes. Also, new bone can be induced to form heterotopically, such as when the BMP are implanted in muscle in animal models using appropriate delivery systems. These observations suggest that BMP could be applied clinically to promotion of repair of bone.

BMP were first characterized in 1965 by Urist as a biologically active molecule inducing new ectopic bone formation from decalcified bone matrix in vivo [14]. A cDNA encoding BMP was cloned by Wozney

in 1988, and BMP were found to be a dimeric protein with a molecular weight of about 32,000 [15–17]. An important common feature of the BMP molecules is the position of cysteine residues in relation to the carboxyl terminus. The positions of these seven cysteine residues are the same as those in transforming growth factor (TGF)-β, indicating that BMP molecules are members of the TGF-β superfamily [18]. Today, the BMP family consists of about 15 BMP [19].

BMP include bone formation during embryogenesis, growth, and adulthood. In fracture healing, osteoprogenitor cells can respond to BMP and differentiate into osteoblasts. BMP bind to their receptors on progenitor cells, initiating signal transduction according to the following sequence. BMP molecules bind to a type IA or IB BMP receptor (BMPR-I) and to a type II BMP receptor (BMPR-II) to form a heterotetramer. These receptors are of the serine/threonine kinase type. As a result of BMP binding, BMPR-II phosphorylate the glycine/serine-rich domain of BMPR-I. BMPR-I then phosphorylate the C-terminal domain of Smads 1, 5, and 8. [Smads is a term identifying homologues of "Mothers against decapentaplegic" (Mad) and the related genes, Sma.] Smad 6 blocks the phosphorylation cascade by binding to BMPR-I. Following phosphorylation, Smads bind to Smad 4 and translocate to the nucleus. On the other hand, when Smads bind to Smad 6, the signal is terminated. Once inside the osteoblast nucleus, Smads initiate and activate Smad target gene transcription [20–22].

Among members of the BMP family, BMP-2, -4, and -7 possess a strong ability to induce bone formation. These BMP molecules have been synthesized successfully by DNA recombination techniques; the protein products (rBMP) have been shown to possess the bone-inducing effect of BMP [23,24]. Thus, human-type BMP (rhBMP) have become available for potential medical use. A number of preclinical studies have assessed the efficacy of rhBMP in healing of bone defects and acceleration of fracture healing.

2.2. Delivery systems for BMP

New bone formation in vivo cannot be obtained simply by injecting aqueous BMP solutions into the area where bone is needed. Delivery systems that retain BMP and release it slowly, as well as serving as scaffolding for new bone formation, are essential. A delivery system also must be biocompatible and biodegradable; lack immunogenicity, toxicity, and carcinogenicity; permit the biologic activity of BMP; be easily handled; be sterilizble; and be inexpensive to produce commercially. A large number of materials that satisfy these conditions have been considered as BMP delivery systems and tested in animals.

One of the first candidate materials was demineralized bone matrix (DBM), from which BMP were originally isolated [14,25]. Osteoconductive delivery systems have included collagenous materials, such as type I collagen (as sponges, gels, or fibrils) [19,26–30], and type IV collagen [31,32]; inorganic ceramic materials, such as hydroxyapatite (HA) (as a powder, granules, or blocks) [33,34], tricalcium phosphate (TCP) [35], glass ceramic, and other inorganic materials; cartilage- or bone-derived materials, such as coral, chitin, and bone mineral; and composites of different types of these materials [20]. BMP have also been used in combination with titanium and other metal alloys [36].

Among these candidates, the most effective material is type I collagen, which now is considered the "gold standard." Type I collagen, a biologically occurring polymer, is a major component of bone and a suitable scaffold. In addition, collagen is degraded and absorbed in vivo, allowing its disappearance after new bone is formed. Since this collagen was extracted from tendons and skin of pigs and cattle, an atelocollagen was developed from these sources largely eliminating antigenicity. In animal tests, many excellent results have been obtained using this collagen with BMP. This atelocollagen delivery system also is used for clinical trials of BMP but some antigenicity remains, posing a degree of risk of immunologic reaction when used repetitively or in large amounts. Furthermore, a potential risk exists for transmission of infectious disease [37–39]. Finally, biodegradability and other properties are difficult to adjust. To avoid these problems, synthetic degradable polymers have been examined as possible BMP delivery systems.

2.3. Synthetic polymers for BMP delivery system

Synthetic biodegradable polymers pose no danger of immunogenicity or possibility of disease trans-

mission. In addition, characteristics such as strength, degradability, and adhesiveness can be altered to facilitate clinical use.

Biodegradable polymers with high biocompatibility originated in the development of suture materials for surgery. These materials must be strong immediately after the operation when the tissue is sutured in vivo, but after the wound has healed, they ideally should degrade and be absorbed. For this purpose, many biodegradable polymeric suture materials with high biocompatibility have been developed, and large-scale screening tests were carried out. As a result, several kinds of synthetic polymeric suture material are now in clinical use. These include poly-α-hydroxy acids such as polylactic acid (PLA), polyglycolic acid (PGA), and their copolymers (PLAGA). Their favorable characteristics as suture materials has prompted researchers to test their suitability as carriers for BMP.

BMP have been tested with a variety of biodegradable polymers including PLA, PGA, and PLAGA, and other polymers such as polyethylene glycol, poly-ε-caprolactone, and polyphosphazetes [40–46]. However, none has proven equal to collagen [47,48]. We therefore sought to develop new synthetic biodegradable polymers that would prove superior to collagen as BMP delivery system [49–52].

3. Development of new synthetic biodegradable polymers for rhBMP-2 delivery

3.1. Poly-D,L-lactic acid-polyethylene glycol block copolymer (PLA-PEG)

Among rhBMP, we tested rhBMP-2, which has been considered to possess greatest osteoinductive activity. First we tested biodegradable polymers for rhBMP-2 delivery that exhibited plasticity at room temperature. We synthesized PLA-PEG block copolymers of various molecular sizes with various PLA/PEG ratios (Fig. 1) [53,54]. Results were assessed in vivo by mixing each polymer with rhBMP-2 and implanting the mixture into the back muscles of mice for 3 weeks to determine its capacity to induce ectopic bone formation. The results showed superiority of a PLA-PEG block copolymer with a total molecular weight of approximately 9500 and a PLA/PEG molar ratio of approximately 3:2. Although this polymer worked well as a delivery system for rhBMP-2 and new ectopic bone was induced consistently, degradation of this polymer was somewhat slow; the material remained at the center of the rhBMP-2-induced ossicles.

PLA-PEG

$$\underbrace{H\text{-}(\text{-}O\text{-}CH(CH_3)\text{-}CO\text{-})_m}_{\text{PLA segment}}\text{-}O\text{-}\underbrace{(\text{-}CH_2\text{-}CH_2\text{-}O\text{-})_n}_{\text{PEG segment}}\text{-}\underbrace{(\text{-}OC\text{-}CH(CH_3)\text{-}O\text{-})_o\text{-}H}_{\text{PLA segment}}$$

PLA-DX-PEG

$$\underbrace{H\text{-}(\text{-}O\text{-}CH(CH_3)\text{-}CO\text{-})_m\text{-}(\text{-}O\text{-}CH_2\text{-}CH_2\text{-}O\text{-}CH_2\text{-}CO\text{-})_n}_{\text{PLA-DX random polymer segment}}\text{-}O\text{-}\underbrace{(\text{-}CH_2\text{-}CH_2\text{-}O\text{-})_o}_{\text{PEG segment}}\text{--}$$

$$\text{--}\underbrace{(\text{-}OC\text{-}CH_2\text{-}O\text{-}CH_2\text{-}CH_2\text{-}O\text{-})_p\text{-}(\text{-}OC\text{-}CH(CH_3)\text{-}O\text{-})_q\text{-}H}_{\text{PLA-DX random polymer segment}}$$

Fig. 1. Structural formulas of poly-D,L-lactic acid-polyethylene glycol block copolymer (PLA-PEG) and poly-D,L-lactic acid-p-dioxanone-polyethylene glycol block copolymer (PLA-DX-PEG). Both are A–B–A type polymers. m, n, o, p, q: number of units.

3.2. Poly-D,L-lactic acid-para-dioxanone-polyethylene glycol block copolymer (PLA-DX-PEG)

To optimize degradation of the polymer used to deliver rhBMP-2, para-dioxanone molecules were randomly inserted into the PLA segments of the PLA-PEG polymer without changing the total molecular weight [55]. This PLA-DX-PEG block copolymer represents a novel material (Fig. 1). Use of this new polymer as a delivery system for rhBMP-2 resulted in complete replacement of the implants by new bone with no visible remnants of the polymer, presumably reflecting a favorable degradation rate. In vivo comparison showed that the rhBMP-2/PLA-DX-PEG composite implants could induce new bone formation more effectively than a PLA-PEG/rhBMP-2 composite.

PLA-DX-PEG consists of a copolymer of polylactic acid and para-dioxanone and a homopolymer of polyethylene glycol. Individually, these polymers already have been used clinically as suture materials, screws, and delivery systems for other drugs. Therefore, PLA-DX-PEG is anticipated to be safe for clinical use as well. Nevertheless, further tests in large animals or primates are essential before this bone-inducing implant can be studied in a clinical setting. At room temperature, PLA-DX-PEG with molecular weight of 9500 is a firm gel that is easy to manipulate (Fig. 2). We tested whether this novel polymer could act as an effective rhBMP-2 delivery system.

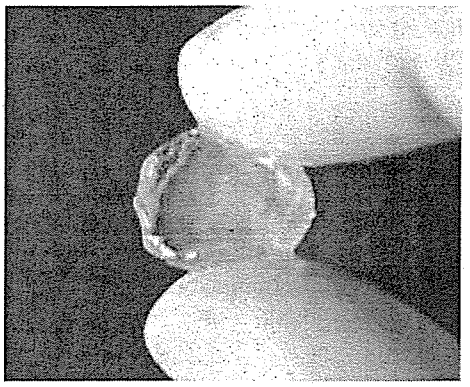

Fig. 2. Appearance of PLA-DX-PEG (reprinted from [51], with permission from Marcel Dekker Inc.) requires copyright permission since we previously published in Tissue engineering and novel delivery systems [51]. At room temperature, PLA-DX-PEG with a molecular weight of 9500 is a firm gel, which can be shaped and is easy to manipulate.

The PLA-DX-PEG polymer mass was dissolved in organic solvent (acetone) and mixed with rhBMP-2 solution. After agitation, acetone was removed by evaporation with a centrifuge evaporator to return the polymer to its native state (Fig. 3). Male ddy mice (5 weeks old) were anesthetized with diethyl ether, and test implants were aseptically placed into the left dorsal muscle pouches (one per animal). Three weeks after surgery, the implants were harvested together with surrounding tissues. Soft X-ray radiographs and histologic examination of ectopic new bone showed mature trabecular bone and hematopoietic bone marrow (Fig. 4). No evidence of inflammatory or foreign-body reaction from the host could be found in tissues adjacent to the new bone.

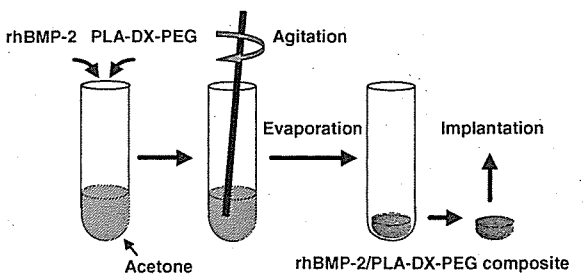

Fig. 3. Methods for combining PLA-DX-PEG polymer with rhBMP-2. PLA-DX-PEG was dissolved in organic solvent, and rhBMP-2 solution was mixed in it. Evaporation with a centrifuge evaporator removed the solvent, so an rhBMP-2/PLA-DX-PEG composite implant was obtained.

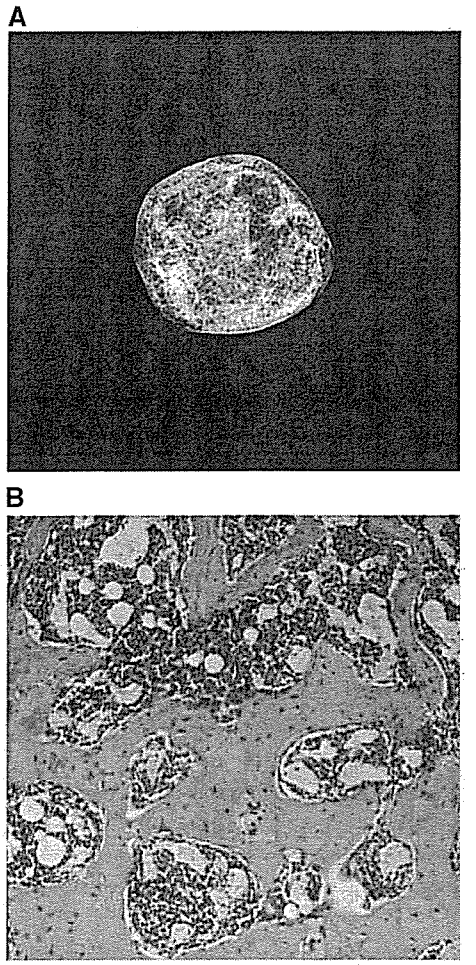

Fig. 4. Ectopic bone formation induced by the rhBMP-2/PLA-DX-PEG composite (reprinted from [55], with permission from Nature Publishing Group) requires copyright permission since we previously published in Nat. Biotechnol. [55]. The composite was placed in the back muscle of mouse, which was harvested after 3 weeks. Ectopic new bone showed mature bone trabeculae with hematopoietic bone marrow. (A) Soft X-ray radiograph. (B) Photomicrograph. Hematoxylin and eosin stain.

We compared the PLA-DX-PEG polymer and collagen as rhBMP-2 delivery systems. For a positive control implant, an aliquot of rhBMP-2 solution was absorbed by a type I collagen sponge disc, lyophilized, and compressed to form an implant of the same volume as the PLA-DX-PEG implant. As a result, implants containing more than 0.5 μg of rhBMP-2 showed bone formation in both groups. Therefore, in terms of ability to elicit new bone formation by rhBMP-2, the PLA-DX-PEG delivery system was

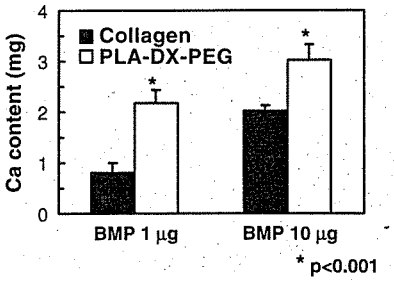

Fig. 5. Comparison of calcium content of new bone obtained using an PLA-DX-PEG system and a collagen system (reprinted from [55], with permission from Nature Publishing Group) requires copyright permission since we previously published in Nat. Biotechnol. [55]. The calcium content of new bone obtained using the PLA-DX-PEG system was significantly higher than that obtained using the collagen system for both 1 μg and 10 μg of rhBMP-2.

equal to the collagen system. Amounts of calcium in the new bones induced in the PLA-DX-PEG and the collagen delivery system groups with 1 μg or 10 μg of rhBMP-2 were quantified. The mean calcium content in ossicles from the PLA-DX-PEG group was significantly higher than in those from the collagen group at both doses (Fig. 5). Therefore, this polymeric delivery system may permit reduction of the effective dose of rhBMP-2 for clinical use compared to doses used with collagen.

4. Repair of bone tissues using rhBMP-2 and new synthetic polymers

4.1. Repair of bone defect using composites of rhBMP-2 and synthetic polymers

Use of rhBMP-2 in combination with a delivery system material ideally forms new bone of the same shape as that of the original bone. Development of synthetic biodegradable polymers is believed to permit control of the size and shape of newly formed bone if an appropriate delivery system is used. For this purpose, the hard gel type of PLA-DX-PEG is suitable [55].

To test whether this novel polymer functions appropriately in large bone defects in vivo, we implanted rhBMP-2/PLA-DX-PEG composites in rat iliac bone defects 4 mm in diameters, which is considered a critical size for informative testing. We examined these defects using radiographic and histologic methods. The bone defect was repaired in a manner showing rhBMP-2 dose dependence and time dependence. Histologic analysis of the specimens revealed that defects treated with 10 μg of rhBMP-2 were filled with dense trabecular bone with no evidence of polymer remnants at 4 weeks post-operatively. At the host–defect interface, new bone had formed adjacent to the host bone (Fig. 6). These

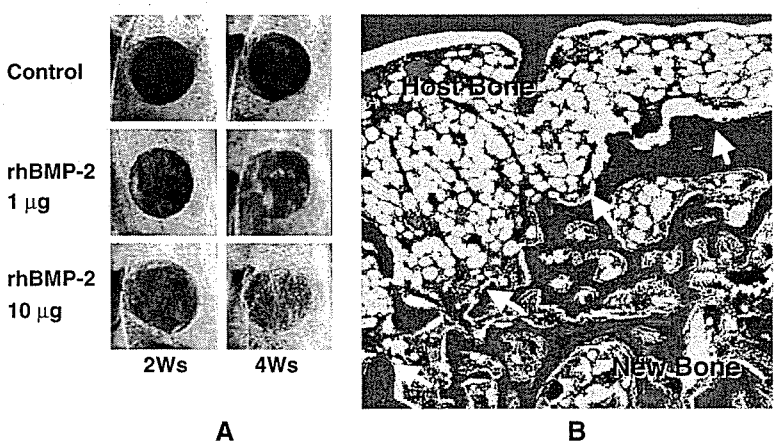

Fig. 6. Repair of a bone defect using PLA-DX-PEG as a delivery system for rhBMP-2 (reprinted from [55], with permission from Nature Publishing Group) requires copyright permission since we previously published in Nat. Biotechnol. [55]. A cylindrical defect 4 mm in diameter was created in the ilium of rats, and was filled with rhBMP-2/PLA-DX-PEG composite. (A) The defect was repaired with newly formed bone in a manner dependent on rhBMP-2 dose and on time. (B) New bone with hematopoietic marrow and bony trabeculae was formed adjacent to the host bone (arrows). Hematoxylin and eosin stain.

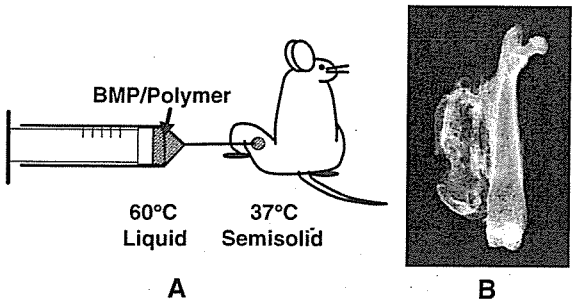

Fig. 7. Injectable polymeric delivery system for rhBMP-2 (reprinted from [56], with permission from Elsevier) requires copyright permission since we previously published in Bone [56]. (A) When heated to 60 °C, the rhBMP-2/PLA-DX-PEG composite can be injected percutaneously, avoiding need for surgical implantation. Subsequently, implants become firm upon cooling to body temperature, resulting in semisolid polymeric implants in vivo. (B) Soft X-ray radiograph of new orthotopic bone formed by injection of the rhBMP-2/PLA-DX-PEG composite in the muscle pouch on the abraded surface of the murine femur 3 weeks after injection.

results suggest that rhBMP-2 in the PLA-DX-PEG polymer delivery system should be suitable for eliciting bone formation and healing in large bone defects.

4.2. Injectable polymeric delivery systems for rhBMP-2

Injectable delivery systems for rhBMP-2 could provide a less invasive method for repair of bone defects, avoiding extensive invasive surgery [56]. Clinical indications might include fresh fractures, nonunion, or delayed union of bone causing serious difficulty in fracture treatment, as well as large defects often associated with bone tumor resection. As far as we know, no such delivery system has been developed or reported.

The new synthetic biodegradable PLA-DX-PEG polymers feature an exquisite temperature-dependent liquid–semisolid transition and work well as an injectable rhBMP-2 delivery system. The thermosensitive property of the rhBMP-2/PLA-DX-PEG composite permits percutaneous injection after heating. Fluidity of the composite decreases as it cools to body temperature, and the resultant semisolid form provides a scaffold for bone formation as it gradually releases rhBMP-2 into its immediate surroundings.

The rhBMP-2 molecule is a heat-stable protein [57]. For example, biologic activity of rhBMP-2 was unchanged after heating to 60 °C for 30 min. Considering the heat-stable character of rhBMP-2, PLA-DX-PEG with molecular weight of 6400 could be a suitable system for injectable delivery of rhBMP-2. Together with rhBMP-2, this polymer heated to 60 °C could be injected as a liquid and then turn to a semisolid form in vivo at 37 °C. The properties of the polymer would allow retention of BMP for a period of time sufficient to elicit new bone formation while serving as a scaffold for further bone growth. Eventually, it would be completely replaced by new bone, avoiding surgery for removal since the polymer is biodegradable (Fig. 7A). To further demonstrate the efficacy of this polymer, 25 mg of PLA-DX-PEG mixed with 10 μg of rhBMP-2 was heated at 60 °C for 5 min and injected using a 14-gauge needle into muscle overlying the surface of the murine femur. Three weeks after injection, new bone was found at the injection site, and was attached to the surface of the femur (Fig. 7B). This new type of injectable osteoinductive material should allow less invasive surgery involving restoration or repair of bone.

We also tested this injection technique in spinal fusion [58]. The rhBMP-2/PLA-DX-PEG composites were injected into the anterior longitudinal ligaments

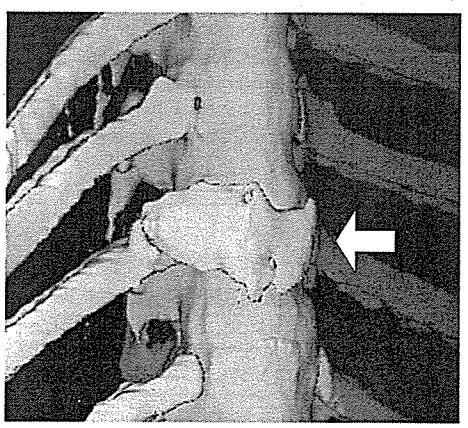

Fig. 8. Spinal fusion by injection of the rhBMP-2/PLA-DX-PEG composite (reprinted from [58], with permission from Lippincott Williams and Wilkins) requires copyright permission since we previously published in J. Spinal Disord. [58]. PLA-DX-PEG with rhBMP-2 was injected into the anterior longitudinal ligament of the spine in dogs. New bone was formed on the anterior aspects of vertebrae after 6 weeks (3D-CT, arrow).

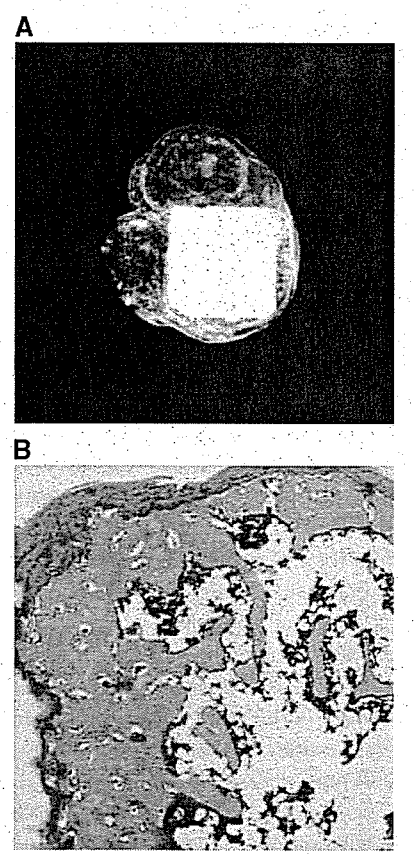

Fig. 9. Ectopic bone formation by hydroxyapatite (HA) with the rhBMP-2/PLA-DX-PEG (reprinted from [54], with permission from The Journal of Bone and Joint Surgery, Inc.) requires copyright permission since we previously published in J. Bone Joint Surg. Am. [54]. The rhBMP-2/PLA-DX-PEG composite was placed in the pores the HA block, which was inserted in the back muscle of mice. (A) Soft X-ray radiograph showed the new bone surrounding HA at 3 weeks. (B) Histologic examination also showed new bone within the pores of the HA.

of the canine spine. Six weeks later, new bone had formed, bridging between the vertebrae anteriorly (Fig. 8). If a pneumoscopic technique were used jointly, anterior spinal fusion might be accomplished by a less invasive approach.

4.3. Combination of the rhBMP-2/polymer composites with other materials

The hydrophilic nature of the PLA-DX-PEG polymer causes it to swell on contact with water. This physical property provides an additional advantage for use of the polymer in combination with porous materials. When a solid implant with pores filled with the rhBMP-2/PLA-DX-PEG composite is implanted, the composite will swell, extruding itself from the pores to form a layer of composite.

To test this property, a combination of the rhBMP-2/PLA-DX-PEG composite with porous hydroxyapatite (HA) was used [54]. The rhBMP-2/PLA-DX-PEG composite was placed in the pores of an HA block, which then was inserted into the back muscle of mice. Over 3 weeks, new bone had formed to surround the HA. Histologic examination showed new bone formation within the pores of the HA as well (Fig. 9).

Next, rhBMP-2 (120 μg) was mixed with the polymer (120 mg) and impregnated into titanium fiber-mesh cylinders [59]. Three 5-mm cylinders were placed end-to-end to fill a 15-mm defect created in the humerus of adult rabbits and stabilized with an intramedullary rod. In controls, the titanium fiber-mesh cylinders contained the polymer but not rhBMP-2. Six weeks after implantation, new bone had formed on the surface of the implant and had bridged the

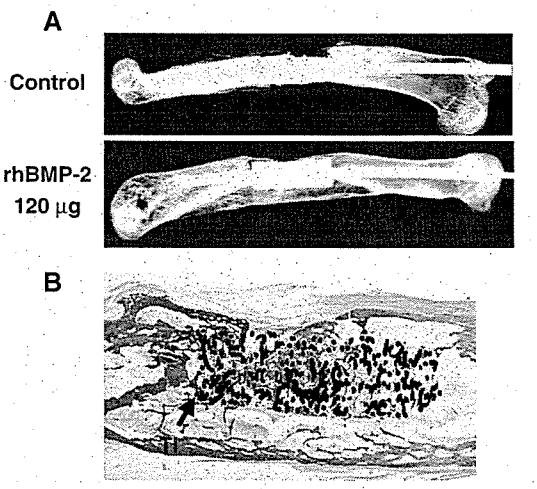

Fig. 10. Repair of a bone defect with a titanium syringe implant with the rhBMP-2/PLA-DX-PEG composite (reprinted from [59], with permission from 6 Wiley) requires copyright permission since we previously published in J. Biomed. Mater. Res. [59]. A bone defect of 1.5 cm was created in the humerus of rabbits, and three 5-mm implants were placed in it. These were stabilized with an intramedullary rod. (A) While the bone defect was not repaired in control groups, the defect was restored in the 120 μg rhBMP-2 group after 5 weeks. (B) Histologic examination showed that new bone also had formed within the titanium mesh (Ti), and that new bone had formed adjacent to the host bone. Hematoxylin and eosin stain.

defect. Defects treated with control implants were not repaired (Fig. 10). These results provide strong evidence that composite implants using rhBMP-2, synthetic degradable polymers, and compatible materials provide enhanced regenerative potential for the repair of a large bone defect. These techniques can repair bones whose function requires great strength, as a combination of rhBMP-2/PLA-DX-PEG composite with HA or titanium represents a mechanically durable osteoinductive material.

4.4. Development of a new artificial joint that restores a bone defect

Total hip arthroplasty (THA) has become essentially the standard procedure for treatment of various hip lesions. However, one limitation of this operation has been the eventual loosening of the prosthesis from periprosthetic bone loss. At revision surgery, various degrees of bone defect, both in the proximal femur and the acetabulum, often are encountered; these present challenges for sufficiently solid fixation of a new prosthesis. Alternative approaches aimed at overcoming this problem have included special design of the revision prosthesis and allo- or autogeneic bone grafting in combination with or without materials such as hydroxyapatite. If such bone loss can be repaired with use of rhBMP-2, revision surgery might be made more effective.

To address the problem of loosening of the prosthesis, we developed a new prosthesis combined with rhBMP-2/PLA-DX-PEG composite [60]. We tested efficacy of the rhBMP-2-containing prosthesis in reconstructing a bone defect in a canine model where the medial half of the proximal femur was resected to create a defect that was repaired with rhBMP-2/PLA-DX-PEG composite. Twelve weeks after implantation, the original bone defects in the rhBMP-2 treatment groups showed repair (Fig. 11). Thus, this type of hybrid prosthesis may represent a new modality for repair of bone defects or restoration of lost bone mass encountered in revision arthroplasty.

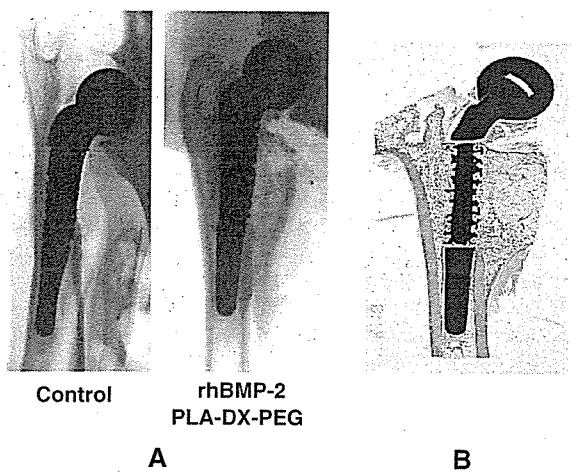

Fig. 11. Repair of a periprosthetic bone defect using PLA-DX-PEG/rhBMP-2 composite adherent to the prosthesis (reprinted from [60], with permission from Elsevier) requires copyright permission since we previously published in Biomaterials [60]. (A) Twelve weeks after implantation, the implant with rhBMP-2/PLA-DX-PEG showed new bone formation at the defect site. In the control group without rhBMP-2, only a scant amount of new bone was seen at the cut ends of the defects, which were not repaired. (B) By microscopic examination of sections in the rhBMP-2 treatment group, the new bone on the surface of implants showed normal histology with hematopoietic marrow and bony trabeculae. New bone formation also was observed within the pores of the titanium mesh. Hematoxylin and eosin stain.

5. Conclusions

A new delivery system using PLA-DX-PEG enabled creation of various osteoinductive materials that could be used to heal fractures and repair large bone defects. Importantly, this new rhBMP-2 delivery system was developed using synthetic biodegradable polymers, avoiding potential risks of disease transmission or immunogenicity associated with use of animal collagen or allogeneic bone grafts. Moreover, this system avoids problems of autogenous bone grafts such as limited supply of donor bone and the need for additional surgery to harvest the bone, with the risk of additional morbidity.

In summary, this new rhBMP-2 delivery system represents an innovative potential therapy that is safe, efficacious, and less invasive than current approaches for repair of damaged bone. Further work will be necessary to determine whether the biocompatible and biodegradable properties exhibited by the PLA-DX-PEG polymers in these studies are replicated during the practical application of rhBMP-2 in patient care.

Acknowledgements

This work was supported by a Grant-in-Aid for Scientific Research from the Ministry of Education, Science, Sports and Culture, Japan, a Grant of Japan Rheumatism Foundation, a Grant from Hip Joint Foundation of Japan, a Grant from Japan Orthopaedics and Traumatology Foundation Inc., a Grant from NOVARTIS Foundation (Japan) for the Promotion of Science, and a Grant from TERUMO Life Science Foundation.

References

[1] T.S. Einhorn, Enhancement of fracture-healing, J. Bone Jt. Surg., Am. 77 (1995) 940–956.
[2] S.M. Doppelt, W.W. Tomford, A.B. Lucas, H.J. Mankin, Operational and financial aspects of a hospital bone bank, J. Bone Jt. Surg., Am. 63 (1981) 1472–1481.
[3] T.I. Malinin, O.V. Martinez, M.D. Brown, Banking of massive osteoarticular and intercalary bone allografts: 12 years' experience, Clin. Orthop. 197 (1985) 44–57.
[4] J.A. Memzek, S.P. Arnoczky, C.L. Swenson, Retroviral transmission by the transplantation of connective-tissue allografts, J. Bone Jt. Surg., Am. 76 (1995) 1034–1041.
[5] E. Canalis, Effect of growth factors on bone cell replication and differentiation, Clin. Orthop. 193 (1985) 246–263.
[6] A.H. Reddi, Symbiosis of biotechnology and biomaterials: application in tissue engineering of bone and cartilage, J. Cell. Biochem. 56 (1994) 192–195.
[7] U. Ripamonti, A.H. Reddi, Tissue engineering, morphogenesis, and regeneration of the periodontal tissues by bone morphogenetic proteins, Crit. Rev. Oral Biol. Med. 8 (1997) 154–163.
[8] J. Fang, Y.Y. Zhu, E. Smiley, J. Bonadio, J.P. Rouleau, S.A. Goldstein, L.K. McCauley, B.L. Davidson, B.J. Roessler, Stimulation of new bone formation by direct transfer of osteogenic plasmid gene, Proc. Natl. Acad. Sci. U. S. A. 93 (1996) 5753–5758.
[9] J. Bonadio, E. Smiley, P. Patil, S. Goldstein, Localized, direct plasmid gene delivery in vivo: prolonged therapy results in reproducible tissue regeneration, Nat. Med. 5 (1999) 753–759.
[10] A.I. Caplan, Mesenchymal stem cells, J. Orthop. Res. 9 (1991) 641–650.
[11] S.E. Haynesworth, J. Goshima, V.M. Goldberg, A.I. Caplan, Characterization of cells with osteogenic potential from human marrow, Bone 13 (1992) 81–88.
[12] H. Ohgushi, Y. Dohi, T. Toshikawa, S. Tamai, S. Tabata, Y. Suwa, In vitro bone formation by rat marrow cell culture, J. Biomed. Mater. Res. 32 (1996) 341–348.
[13] S. Tamura, H. Kataoka, Y. Matsui, Y. Shionoya, K. Ohno, K.I. Michi, K. Takahashi, A. Yamaguchi, The effects of transplantation of osteoblastic cells with bone morphogenetic protein (BMP)/carrier complex on bone repair, Bone 29 (2001) 169–175.
[14] M.R. Urist, Bone formation by autoinduction, Science 150 (1965) 893–899.
[15] J.M. Wozney, V. Rosen, A.J. Celeste, L.M. Mitsock, M.J. Whitters, R.W. Kriz, R.M. Hewick, E.A. Wang, Novel regulators of bone formation: molecular clones and activities, Science 242 (1988) 1528–1534.
[16] K. Takaoka, H. Yoshikawa, J. Hashimoto, S. Miyamoto, K. Masuhara, H. Nakahara, M. Matsui, K. Ono, Purification and characterization of a bone-inducing protein from a murine osteosarcoma (Dunn type), Clin. Orthop. 292 (1993) 122–129.
[17] K. Takaoka, H. Yoshikawa, J. Hashimoto, K. Masuhara, S. Miyamoto, S. Suzuki, K. Ono, M. Matsui, S. Oikawa, N. Tsuruoka, Y. Tawaragi, C. Inuzuka, T. Katayama, M. Sugiyama, M. Tsujimoto, T. Nakanishi, H. Nakazatio, Gene cloning and expression of a bone morphogenetic protein derived from a murine osteosarcoma, Clin. Orthop. 294 (1994) 344–352.
[18] A.J. Celeste, J.A. Iannazzi, R.C. Taylor, R.M. Hewick, V. Rosen, E.A. Wang, J.M. Wozney, Identification of transforming growth factor β family members present in bone inductive protein purified from bovine bone, Proc. Natl. Acad. Sci. U. S. A. 87 (1990) 9843–9847.
[19] M. Geiger, R.H. Li, W. Friess, Collagen sponges for bone regeneration with rhBMP-2, Adv. Drug Deliv. Rev. 55 (2003) 1613–1629.
[20] C.A. Kirker-Head, Potential applications and delivery strategies for bone morphogenetic proteins, Adv. Drug Deliv. Rev. 43 (2000) 65–92.
[21] T. Sakou, Bone morphogenetic proteines: from basic studies to clinical approaches, Bone 22 (1998) 591–603.
[22] J.M. Schmitt, K. Hwang, S.R. Winn, J.O. Hollinger, Bone morphogenetic proteins: an update on basic biology and clinical relevance, J. Orthop. Res. 17 (1999) 269–278.
[23] E.A. Wang, V. Rosen, Recombinant human bone morphogenetic protein induces bone formation, Proc. Natl. Acad. Sci. U. S. A. 87 (1990) 2220–2224.
[24] J.M. Wozney, The bone morphogenetic protein family and osteogenesis, Mol. Reprod. Dev. 32 (1992) 160–167.
[25] T.K. Sampath, J.E. Coughlin, R.M. Whetstone, D. Banach, C. Corbett, R.J. Ridge, E. Ozkaynak, H. Oppermann, D.C. Rueger, Bovine osteogenic protein is composed of dimers of OP-1 and BMP2A, two members of the transforming growth factor beta superfamily, J. Biol. Chem. 265 (1990) 13198–13250.
[26] K. Takaoka, M. Koezuka, H. Nakahara, Telopeptide-depleted bovine skin collagen as a carrier for bone morphogenetic protein, J. Orthop. Res. 9 (1991) 902–907.
[27] S.D. Cook, M.W. Wolfe, S.L. Salkeld, D.C. Rueger, Effect of recombinant human osteogenic protein-1 on healing of segmental defects in non-human primates, J. Bone Jt. Surg., Am. 77 (1995) 734–750.
[28] J.H. Schimandle, S.D. Boden, W.C. Hutton, Experimental spinal fusion with recombinant human bone morphogenetic protein-2, Spine 20 (1995) 1326–1337.

[29] U. Ripamonti, M. Heliotis, D.C. Rueger, T.K. Sampath, Induction of cementogenesis by recombinant human osteogenic protein-1 (hOP-1/BMP-7) in the baboon (*Papio ursinus*), Arch. Oral Biol. 41 (1996) 121–126.
[30] H. Itoh, S. Ebara, M. Kamimura, Y. Tateiwa, T. Kinoshita, Y. Yuzawa, K. Takaoka, Experimental spinal fusion with use of recombinant human bone morphogenetic protein 2, Spine 24 (1999) 1402–1405.
[31] V.V. Viljanen, T.J. Gao, T.C. Lindholm, T.S. Lindholm, B. Kommonen, Xenogeneic moose (*Alces alces*) bone morphogenetic protein (mBMP)-induced repair of critical-size skull defects in sheep, Int. J. Oral Maxillofac. Surg. 25 (1996) 217–222.
[32] T.J. Gao, T.S. Lindholm, B. Kommonen, P. Ragni, A. Paronzini, T.C. Lindholm, T. Jamsa, P. Jalovaara, Enhanced healing of segmental tibial defects in sheep by a composite bone substitute composed of tricalcium phosphate cylinder, bone morphogenetic protein, and Type IV collagen, J. Biomed. Mater. Res. 32 (1996) 505–512.
[33] E. Tsuruga, H. Takita, H. Itoh, Y. Wakisaka, Y. Kuboki, Pore size of porous hydroxyapatite as the cell-substratum controls BMP-induced osteogenesis, J. Biochem. 121 (1997) 317–324.
[34] J.A. Koempel, B.S. Patt, K. O'Grady, J. Wozney, D.M. Toriumi, The effect of recombinant human bone morphogenetic protein-2 on the integration of porous hydroxyapatite implants with bone, J. Biomed. Mater. Res. 41 (1998) 59–63.
[35] D.D. Lee, A. Tofighi, M. Aiolova, P. Chakravarthy, A. Catalano, A. Majahad, D. Knaack, Alpha-BSM: a biomimetic bone substitute and drug delivery vehicle, Clin. Orthop. 367 (1999) S396–S405.
[36] B.J. Cole, M.P. Bostrom, T.L. Pritchard, D.R. Sumner, E. Tomin, J.M. Lane, A.J. Weiland, Use of bone morphogenetic protein 2 on ectopic porous coated implants in the rat, Clin. Orthop. 345 (1997) 219–228.
[37] F.H. Bach, J.A. Fishman, N. Daniels, J. Proimos, B. Anderson, C.B. Carpenter, L. Forrow, S.C. Robson, H.V. Fineberg, Uncertainty in xenotransplantation: individual benefit versus collective risk, Nat. Med. 4 (1998) 141–144.
[38] D. Butler, M. Wadman, S. Lehrman, Q. Schiermeier, Last chance to stop and think on risks of xenotransplants, Nature 391 (1998) 320–324.
[39] F. DeLustro, J. Dasch, J. Keefe, L. Ellingsworth, Immune responses to allogeneic and xenogeneic implants of collagen and collagen derivatives, Clin. Orthop. 260 (1990) 263–279.
[40] J.O. Hollinger, G.C. Battistone, Biodegradable bone repair materials: synthetic polymers and ceramics, Clin. Orthop. 207 (1986) 290–305.
[41] R. Kenley, L. Marden, T. Turek, L. Jin, E. Ron, J.O. Hollinger, Osseous regeneration in the rat calvarium using novel delivery system for recombinant human bone morphogenetic protein-2 (rhBMP-2), J. Biomed. Mater. Res. 28 (1994) 1139–1147.
[42] S.C. Lee, M. Shea, M.A. Battle, K. Kozitza, E. Ron, T. Turek, R.G. Schaub, W.C. Hayes, Healing of large segmental defects in rat femurs is aided by rhBMP-2 in PLGA matrix, J. Biomed. Mater. Res. 28 (1994) 1149–1156.
[43] M.C. Meikle, S. Papaioannou, T.J. Ratledge, P.M. Speight, S.R. Watt-Smith, P.A. Hill, J.J. Reynolds, Effect of poly DL-lactide-co-glycolide implants and xenogeneic bone matrix-derived growth factors on calvarial bone repair in the rabbit, Biomaterials 15 (1994) 513–521.
[44] H.S. Sandhu, L.E.A. Kanim, J.M. Kabo, J.M. Toth, E.N. Zeegen, D. Liu, L.L. Seeger, E.G. Dawson, Evaluation of rhBMP-2 with an OPLA carrier in a canine posterolateral (transverse process) spinal fusion model, Spine 20 (1995) 2669–2682.
[45] M. Bostrom, J.M. Lane, E. Tomin, M. Browne, W. Berberian, T. Turek, J. Smith, J. Wozeney, T. Schildhauer, Use of bone morphogenetic protein-2 in the rabbit ulnar nonunion model, Clin. Orthop. 327 (1996) 272–282.
[46] M. Mayer, J. Hollinger, E. Ron, J. Wozeney, Maxillary alveolar cleft repair in dogs using recombinant human bone morphogenetic protein-2 and polymer carrier, Plast. Reconstr. Surg. 98 (1996) 247–259.
[47] O.M. Bostman, Absorbable implants for the fixation of fracture, J. Bone Jt. Surg., Am. 73 (1991) 148–153.
[48] J.O. Hollinger, K. Leong, Poly(α-hydroxy acids): carriers for bone morphogenetic proteins, Biomaterials 17 (1996) 187–194.
[49] K. Takaoka, N. Saito, S. Miyamoto, H. Yoshikawa, T. Okada, in: Y. Ikada, T. Okano (Eds.), Bone-Inducing Implants: New Synthetic Absorbable Poly-D,L-lactic Acid-Polyethylene Glycol Block Copolymers as BMP-Carriers, Tissue Engineering for Therapeutic Use, vol. 3, Elsevier Science B.V., Amsterdam, 1999, pp. 141–151.
[50] K. Takaoka, S. Miyamoto, N. Saito, T. Okada, in: D.L. Wise (Ed.), New Synthetic Degradable Polymers as Carrier Materials for BMP, Biomaterials Engineering and Devices: Human Applications, vol. 1, The Humana Press, New Jersey, 2000, pp. 239–249.
[51] N. Saito, H. Horiuchi, N. Murakami, J. Takahashi, T. Okada, K. Nozaki, K. Takaoka, in: M.J. Yaszemski, D.J. Trantolo, K.U. Lewandrowski, V. Hasirci, D.E. Altobelli, D.L. Wise (Eds.), New Synthetic Biodegradable Polymers for Bone Morphogenetic Protein Delivery Systems, Tissue Engineering and Novel Delivery Systems, Marcel Dekker Inc., New York, 2004, pp. 475–482.
[52] N. Saito, K. Takaoka, New synthetic biodegradable polymers as BMP carriers for bone tissue engineering, Biomaterials 24 (2003) 2287–2293.
[53] N. Saito, T. Okada, S. Toba, S. Miyamoto, K. Takaoka, New synthetic absorbable polymers as BMP-carriers: plastic properties of poly-D,L-lactic acid-polyethylene glycol block copolymers, J. Biomed. Mater. Res. 47 (1999) 104–110.
[54] N. Saito, T. Okada, H. Horiuchi, N. Murakami, J. Takahashi, M. Nawata, H. Ota, S. Miyamoto, K. Nozaki, K. Takaoka, Biodegradable poly-D,L-lactic acid-polyethylene glycol block copolymers as a BMP delivery system for inducing bone, J. Bone Jt. Surg., Am. 83 (Suppl. 1) (2001) 92–98.
[55] N. Saito, T. Okada, H. Horiuchi, N. Murakami, J. Takahashi, M. Nawata, H. Ota, K. Nozaki, K. Takaoka, A biodegradable polymer as a cytokine delivery system for inducing bone formation, Nat. Biotechnol. 19 (2001) 332–335.
[56] N. Saito, T. Okada, H. Horiuchi, H. Ota, J. Takahashi, N. Murakami, M. Nawata, S. Kojima, K. Nozaki, K. Takaoka,

Local bone formation by injection of recombinant human bone morphogenetic protein-2 contained in polymer carriers, Bone 32 (2003) 381–386.
[57] H. Izawa, Y. Hachiya, T. Kawai, K. Muramatsu, Y. Narita, N. Ban, H. Yishizawa, The effect of heat-treated human bone morphogenetic protein on clinical implantation, Clin. Orthop. 390 (2001) 252–258.
[58] J. Takahashi, N. Saito, S. Ebara, T. Kinoshita, H. Itoh, T. Okada, K. Nozaki, K. Takaoka, Anterior thoracic spinal fusion in dogs by injection of recombinant human bone morphogenetic-2 and a synthetic polymer, J. Spinal Disord. 16 (2003) 137–143.
[59] N. Murakami, N. Saito, H. Horiuchi, T. Okada, K. Nozaki, K. Takaoka, Repair of segmental defects in rabbit humeri with titanium fiber mesh cylinders containing recombinant human bone morphogenetic protein-2 (rhBMP-2) and a synthetic polymer, J. Biomed. Mater. Res. 62 (2002) 169–174.
[60] N. Murakami, N. Saito, J. Takahashi, H. Ota, H. Horiuchi, M. Nawata, T. Okada, K. Nozaki, K. Takaoka, Repair of a proximal femoral bone defect in dogs using a porous surfaced prosthesis in combination with recombinant BMP-2 and a synthetic polymer carrier, Biomaterials 24 (2003) 2153–2159.

RA 肘の運動解析

中村 順之　木村 貞治*　加藤 博之
村上 成道　畑 幸彦

Key Words：Rheumatoid arthritis（関節リウマチ），Movement analysis（運動解析），Accelerometer（加速度計）

【目的】関節リウマチ（以下ＲＡ）肘の運動特性を明らかにする目的で、筋電図、電気角度計、3軸加速度計を用いて、RA 肘と健常肘における屈曲伸展運動の in vivo movement study を行い、両群を比較した。

【対象】肘関節に愁訴、外傷の既往が無く、徒手的に肘関節の不安定性が無いボランティア女性11例（年齢50～74歳、平均62歳）を健常群とした。RA 肘群は、女性患者４例（年齢59～75歳、平均67歳、全例Larsen分類 Grade Ⅳ）であった。全例が人工肘関節置換術施行予定であり、肘屈曲伸展運動で運動時痛を訴えていた。両群ともに右肘関節を測定した。

【方法】

a.　表面筋電図

表面電極をBiceps 、Brachioradialis 、Triceps medial head 、Triceps lateral head 、Anconeous 、Flexor carpi ulnaris 、Pronator teres 、Extensor carpi radialis 、Extensor carpi ulnaris に貼付した。アース電極は肩峰に貼付し、ノイズ防止のためアースシートを使用した。

ｂ．電気角度計（図１）

電気角度形 SG110（バイオメトリクス社、英国）を肘関節内側に設置し、屈曲伸展の運動相を区切った。

ｃ．３軸加速度計（図１）

前腕の回旋を中間位、肘関節９０度屈曲位として３軸加速度計を設置した。加速度計AC101（(株）セプロテック、静岡、日本）は橈骨手根関節面から近位3cmの橈骨茎状突起上の皮膚にテープで固定した。加速度の軸は、手掌方向を肘内反、手背方向を肘外反の加速度変化とした。

ｄ．肘屈曲伸展運動のタイミングの取り方

肘屈曲伸展運動の時間を均一にし、また被検者の運動の指標となるように、timing switch として電子メトロノームを採用した。発光ダイオード光と音に同期して肘の屈曲・伸展運動を行った。

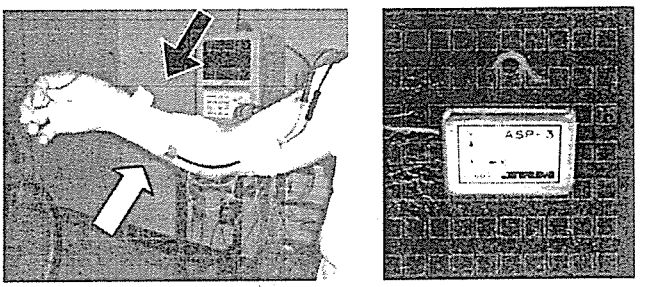

図　1　左：電気角度計（白矢印）、加速度計（黒矢印）の設置　　右：３軸加速度計

e.　測定条件

被検者は背もたれ付き椅子に密着して座らせた。表面筋電図、電気角度計、加速度計を装着し、上腕をバストバンドで体幹に固定した。前腕回旋中間位で肘関節を最大伸展位から最大屈曲位までの屈曲伸展運動を 0.5Hz で行った。10回の屈曲・伸展運動を１セットとした。

ｆ．解析

表面筋電図、電気角度計、３軸加速度計の波形、メトロノーム音声信号を同時にノート型コンピューター内のVITALRECORDER®（㈱キッセイコムテック社、長野、日本）にデータを取り込み、BIMUTAS ®Ⅱ（㈱キッセイコムテック社、長野、日本）で解析を行った。屈曲伸展運動の６回目における最大伸展時より屈曲を開始する時点から屈曲終了の時点までの運動相を「屈曲第６相」とした。以下同様に、第８伸展相までを屈曲相と伸展相に区分した。解析には２セット目のデータを用い、筋電図は屈曲第６～８相を、加速度は屈曲第６相を使用した。筋電図波形は、アーチファクトの影響を除くため10～350Hz でバンドパスフィルターをかけ、re-sampling後に筋電積分値から% MVC を算出した。加速度波形からは、生波形の軌跡、高速フーリエ変換による（Fast Fourier Transform ）周波数解析、さらにre-sampling後の積分値解析を行い、両群を比較した。加速度積分値解析では低い周波数帯域を除外するために10～50Ｈｚでフィルターをかけて算出した。

信州大学整形外科
信州大学医学部保健学科理学療法学 *

【結果】

a. 表面筋電図

% MVC は健常群で Biceps 以外の筋はすべ50%以下であった。健常群では Biceps のみが 3 肘で 52, 54, 57% と 50% 以上を示した。RA 群の% MVC の値で50%以上であった筋は Triceps lateral head 3 肘、Pronator teres 3 肘、Bracihoradialis 2 肘であった。RA 肘の% MVC では特定の筋は健常群に比べ高い値を示す傾向にあった。

b．加速度

健常群は11例中 8 例が屈曲相早期において肘内反方向への加速度が生じ、屈曲後期に肘外反方向へ加速度が移行する傾向を示した。ＲＡ群の加速度生波形には一定の傾向がなかった（図２）。周波数解析ではピークとなる周波数が健常群では 1.9 ～ 8.8Hz 、RA 群で 2.9 ～ 6.8Hz であった。両群の明らかな帯域の差はなかった。加速度積分値では健常群 8.1 ～12.6 G・msec（平均 9.8 ），RA群 4 ～30G・msec（平均14.3 ）でＲＡ群で有意に高い値を示した（＊ｐ＝ 0.002 ）（図３ ）。

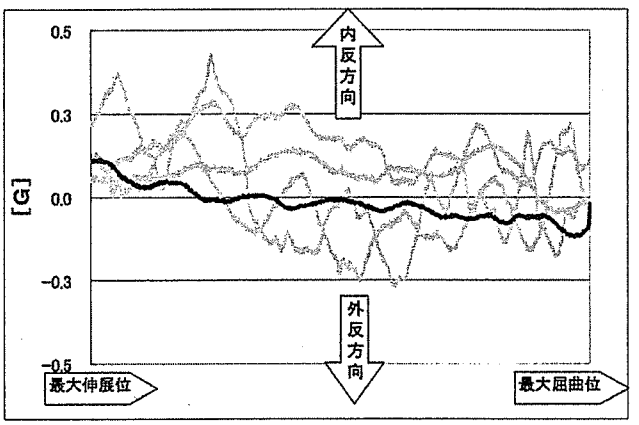

図　2．肘屈曲時　加速度生波形
健常者平均（黒）とＲＡ群各症例（グレー）

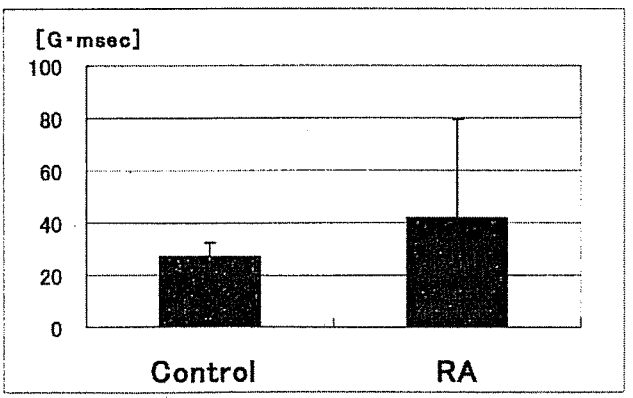

図　3．内外反方向の加速度積分値

【考察】

RA に罹患した関節の movement study を行った研究は少ない。Reddy[1]らにより加速度計を用いた RA 膝患者の運動解析が行われており、また Shah[2] らによって RA ・偽痛風・ spondyloarthropathy 患者の指の運動解析を加速度計で行っているが、肘についてはほとんど行われていない。

今回 RA 肘の in vivo movement study を行ってみると、多くの点で健常肘と測定結果が異なっていた。

表面筋電図解析で健常群より特定の筋で RA 群に高い% MVC が示された。この事実は RA では肘屈曲運動を遂行するには健常より多くの motor unit を動員している可能性がある。あるいは% MVC 算出の基準とした肘関節屈曲伸展の等尺運動時の筋力の低下が関係している可能性もある。

Ｙ軸方向加速度の生波形において、健常群では屈曲早期に内反方向、後期に外反方向の加速度が生じていた。O'Driscoll ら[3] の屍体による肘屈曲運動時の軌跡を測定した研究では、肘屈曲早期で外反位から中間位に向かい、肘屈曲後期で中間位から外反位へ向かう。今回の結果は O'Driscoll らの屍体での実験結果に矛盾しないものであった。周波数解析では傾向の差は明らかにはならなかった。RA 群の測定数が少なく、今後測定数を増やすことで違いが生じる可能性がある。加速度積分値の解析では RA 群で大きい加速度積分値を示した。このことは肘屈曲伸展運動において、健常肘とＲＡ肘が内反外反方向の加速度の周波数帯域が異なることを示している。肘関節の屈曲運動において RA 肘では円滑な運動が障害されている可能性を示している。

【結論】

In vivo movement study を RA 肘に行うことが可能であった。健常肘と RA 肘では、筋活動、関節運動における加速度などの点で異なる傾向があった。今後は対象例を増やすことで RA 肘の運動の特徴、Ｘ線像との関連、人工関節置換術前後の相違などを明らかにする必要がある。

文　献

1) Reddy NP., Noninvasive measurement of acceleration at the knee joint in patients with Rheumatoid Arthritis and Spondyloarthropathy of the Knee . Annals of Biomedical Engineering. 2001;Vol 29,1106-1111

2) Shah EN., Fractal analysis of acceleration signals from patients with CPPD, RA, and spondyloarthropathy of the finger joint. Computer Methods and Programs Biomedicine.2005; 77. 233-239

3)O'Driscoll SW et al. Kinematics of semi-constrained TEA. J Bone Joint Surg Br.1992.74:297-9

4)木藤伸宏．加速度センサーを用いた変形性膝関節症の歩行時下腿運動の解析．　理学療法学. 2004; 31:86-94 .

CLOSED RUPTURE OF THE FLEXOR TENDONS OF THE LITTLE FINGER SECONDARY TO NON-UNION OF FRACTURES OF THE HOOK OF THE HAMATE

H. YAMAZAKI, H. KATO, Y. NAKATSUCHI, N. MURAKAMI and Y. HATA

From the Department of Orthopaedic Surgery, Shinshu University School of Medicine, Matsumoto City, Nagano, Japan and the Department of Orthopaedic Surgery, National Nagano Hospital, Ueda City, Nagano, Japan

We report six patients with closed flexor tendon rupture affecting the little finger, occurring secondarily to non-union of the hook of the hamate bone. The ununited fragments were separated from the basal part of the hook by more than 1 mm. The fragments were also rounded and showed marginal sclerosis. Non-union was located in the middle part of the hook in three patients, the tip in two, and the base in one. At operation, the fragments were removed in all patients. Five patients were treated by free tendon grafts using three palmaris and two plantaris grafts and one underwent tendon transfer. Postoperative total range of active motion of the little finger averaged 218° (range 185–265°). All patients returned to their original employment. This series would suggest that flexor tendon rupture can occur after fracture of the hook of the hamate bone, even when the ununited fragment is small and/or rounded.

Journal of Hand Surgery (British and European Volume, 2006) 31B: 3: 337–341

Keywords: hook of hamate, non-union, flexor tendon, closed rupture

INTRODUCTION

Fractures of the hook of the hamate are rare, accounting for less than 2% of all carpal fractures (Andress and Peckar, 1970; Dunn, 1972). Some of these fractures occur in sports while swinging a baseball bat, golf club, or racquet (Bishop and Beckenbaugh, 1988; Stark et al., 1977). Others are caused by falling on the palm, or by a crush injury to the hand (Bishop and Beckenbaugh, 1988). These fractures are often neglected because routine anteroposterior and lateral roentgenograms of the wrist fail to detect them (Murray et al., 1979; Stark et al., 1989) and disability is minimal, or inapparent, in comparison with other fractures of the carpus. In approximately 14% of hamate hook fractures, non-union of the hook may escape discovery until it, eventually, causes closed rupture of the flexor tendons of the little or ring finger (Boulas and Milek, 1990). To date, 26 such cases of tendon rupture have been reported in the English literature (Bishop and Beckenbaugh, 1988; Boyes et al., 1960; Clayton, 1969; Crosby and Linscheid, 1974; Foucher et al., 1985; Futami et al., 1993; Hartford and Murphy, 1996; Milek and Boulas, 1990; Minami et al., 1985; Stark et al., 1977, 1989; Takami et al., 1983; Teissier et al., 1983; Yang et al., 1996), mostly as case reports. Only six reports have described the site of the fracture (Foucher et al., 1985; Hartford and Murphy, 1996; Milek and Boulas, 1990; Minami et al., 1985; Takami et al., 1983; Yang et al., 1996). No reports have described the roentgenographic features of the non-union of the hook of the hamate associated with the tendon rupture.

This study reviews six cases of closed rupture of the flexor tendons of the little finger secondary to non-union of the hook of the hamate, describing characteristic clinical and roentgenographic features of hook non-union causing tendon rupture. The results of tendon reconstruction in these cases are also discussed.

PATIENTS AND METHODS

Between 1990 and 2002, we treated six patients with closed rupture of the flexor tendons of the little finger secondary to non-union of the hook of the hamate (Table 1). The mean age of the patients was 59 (range 35–73) years. All patients were male. Five were manual labourers and the other was an amateur golfer. In four patients, a mild resistance force applied to the little finger precipitated the rupture; in the other two, rupture apparently occurred spontaneously. One of the latter two patients noted gradual progressive inability to flex the little finger; the other noted, one morning, that he could not flex the little finger. At presentation, four of the patients had palmar pain after attempting to flex the little finger. No patient had difficulty flexing the ring finger and no patient had ulnar nerve palsy. The grip strength was recorded in three patients and was an average of 83% of the strength of the contralateral hand (range 71–90%). Three patients had a past episode of trauma to the palm but none had been diagnosed with hamate fracture at the time. Wrist pain had subsided within 3 months of the injury. Three of the four patients whose rupture was precipitated by force had no symptoms referable to the wrist until tendon rupture occurred. The other patient noted mild pain in the palm while playing golf. The period from palmar injury to tendon rupture ranged from 6 months to 25 years. Two